

Overhead-Aware Design of Reconfigurable Intelligent Surfaces in Smart Radio Environments

Alessio Zappone, *Senior Member IEEE*, Marco Di Renzo, *Fellow IEEE*, Farshad Shams, *Member, IEEE*, Xuewen Qian, *Student Member, IEEE*, Merouane Debbah, *Fellow IEEE*

Abstract

Reconfigurable intelligent surfaces have emerged as a promising technology for future wireless networks. Given that a large number of reflecting elements is typically used, and that the surface has no signal processing capabilities, a major challenge is to cope with the overhead that is required to estimate the channel state information and to report the optimized phase shifts to the surface. This issue has not been addressed by previous works, which do not explicitly consider the overhead during the resource allocation phase. This work aims at filling this gap, developing an overhead-aware resource allocation framework for wireless networks where reconfigurable intelligent surfaces are used to improve the communication performance. An overhead model is developed and incorporated in the expressions of the system rate and energy efficiencies, which are then optimized with respect to the phase shifts of the reconfigurable intelligent surface, the transmit and receive filters, and the power and bandwidth used for the communication and feedback phases. The bi-objective maximization of the rate and energy efficiency is carried out as well. The proposed framework allows characterizing the trade-off between optimized radio resources and the related overhead in networks with reconfigurable intelligent surfaces.

I. INTRODUCTION

Future wireless networks will be a pervasive platform, which will not only connect us but will embrace us through a plethora of services. The ubiquity, speed, and low latency of such networks

A. Zappone is with the University of Cassino and Southern Lazio, Cassino, Italy (alessio.zappone@unicas.it). M. Di Renzo and F. Shams are with the Laboratoire des Signaux et Systèmes, CNRS, CentraleSupélec, Univ. ParisSud, Univ. Paris-Saclay, Gif-sur-Yvette, France ({marco.direnzo, farshad.shams}@l2s.centralesupelec.fr), M. Debbah is with Huawei France R&D, Boulogne-Billancourt, France.

will allow currently disparate devices and systems to become a distributed intelligent communications, sensing, and computing platform [1]. Small-cell networks [2], massive multiple-input-multiple-output systems [3], and millimeter-wave communications [4] are three fundamental technologies that will spearhead the emergence of future wireless networks – Their advantages are undeniable [5]. The question is, however, whether these technologies will be sufficient to meet the requirements of future networks that integrate communications, sensing, and computing in a single platform. Wireless networks, in addition, are rapidly evolving towards a software-defined design paradigm, where every part of the network can be configured and controlled via software [6], [7]. In this optimization process, however, the wireless environment itself, i.e., the medium or channel, is generally assumed to be uncontrollable, and often an impediment to be reckoned with. For example, signal attenuation limits network connectivity, multi-path propagation results in fading phenomena, reflections from objects produce uncontrollable interference.

Motivated by these considerations, the concept of “smart radio environment” has recently emerged [8], [9], [10], wherein the environmental objects are envisioned to be coated with man-made intelligent surfaces of configurable electromagnetic materials that are referred to as reconfigurable intelligent surfaces (RISs) [11], [12]. These materials are expected to contain integrated electronic circuits and software that will enable them to control the wireless medium [10], [13]. Conceptually, an RIS can be viewed as a reconfigurable mirror or lens, depending on its configuration [14], that is made of a number of elementary elements, often referred to as unit-cells or meta-atoms, that are configurable and programmable in software. The input-output response of each unit-cell, in particular, can be appropriately customized, so that, e.g., the signals impinging upon the RIS can be reflected or transmitted towards specified directions or focused towards specified locations [15], [16]. RISs have the potential to enable operators to design the propagation environment, thus potentially changing the design of wireless networks.

Due to the potential opportunities offered by RIS-empowered wireless networks, a large body of research contributions have recently appeared in the literature. The interested readers are referred to the survey papers in [10], [17], [18], [19], [20], where a comprehensive description of the state-of-the-art, the scientific challenges, the distinctive differences with other technologies, and the open research issues are comprehensively discussed. In [21], systems made of large active surfaces are put forth as the natural evolution of massive MIMO systems. A similar idea is embraced in [22], where it is elaborated on how RISs can be used to implement massive MIMO systems, replacing each conventional antenna with an active meta-surface. The fundamental

performance of the system is analyzed, showing that it grants satisfactory performance, while at the same time reducing costs, power consumption, and physical size. In [23] it is shown how RISs can yield better performance compared to the use of relays. Moreover, in [24] it is shown that RISs can improve the secrecy of communication by focusing the transmit signal only towards the direction of the intended receivers. Recently, in addition, a few experimental testbeds have been built to substantiate the feasibility of RISs, e.g., [25], [26], [27], [28], [29]. In the following two sub-sections, we describe the contributions that are most related to the present paper, and outline novelty and contributions of our work.

A. Related Works

We focus our attention on the issue of resource allocation in RIS-empowered wireless networks. In this context, several research papers have appeared recently, mostly considering application scenarios where the line-of-sight link is either too weak or is not available, and, therefore, an RIS is employed to enable the communication through the optimization of the phase shifts of its individual unit-cells and of the precoding and decoding vectors of the transmitter and receiver, respectively. In [30], the rate and energy efficiency are optimized in RIS-based multiple input single output (MISO) downlink systems. Alternating optimization of the base station beamformer and of the RIS phase shifts is performed by means of fractional programming methods for power optimization, and sequential optimization methods for phase optimization. A similar setup is considered in [31], with the difference that the problem of power minimization subject to minimum rate constraints is considered. A suboptimal numerical method is proposed based on alternating optimization. In [32], a MISO downlink system is analyzed, with the addition that the orthogonal frequency division multiplexing (OFDM) transmission scheme is considered, and the problem of sum-rate maximization is addressed. Sum-rate maximization is also investigated in [33], where computationally-efficient, but sub-optimal, algorithms are devised for an RIS-based MISO system, to optimize the transmit beamformer and the RIS phase shifts, still based on the use of alternating optimization. Similarly, alternating optimization methods are used in [34] to tackle the problem of sum-rate maximization in a MISO downlink system. The base station beamformer and the RIS phase shifts are optimized, with the additional difficulty that discrete phase-shifts at the RIS are assumed. In [35], an RIS is used to boost the performance of over-the-air computations in a multi-user MISO channel. A method based on alternating optimization and difference convex (DC)-programming is developed, which outperforms previously proposed

semi-definite relaxation methods. Nevertheless, global optimality can not be guaranteed. In [36], an RIS is used to enhance the secrecy rate of a MISO downlink channel with multiple eavesdroppers. Alternating maximization is used to devise a practical, yet suboptimal, method to optimize the transmit beamformer and the RIS phase shifts. In [37], the use of RISs for physical layer security is envisioned, thanks to the possibility of RISs to reflect incoming signals towards specified directions. In [38], the maximization of the secrecy rate in an RIS-based multiple-antenna system is investigated, and alternating optimization is used to optimize the transmit beamformer and the RIS phase shifts. In [39] a massive MIMO system is considered, in which multiple RISs equipped with a large number of reflectors are deployed and the problem of maximizing the minimum signal-to-interference-plus-noise-ratio at the users is tackled by jointly optimizing the transmit precoding vector and the RISs phase shifts. In [40], it is shown that the use of RISs enhances systems based on unmanned aerial vehicles (UAVs) upon optimizing the UAV height as well as various RIS parameters such as size, altitude, and distance from base station. In [41], the problem of precoding design in an RIS-based multi-user MISO wireless system is addressed, assuming that only discrete phase shifts values at the RIS are possible. The maximization of the rate in an RIS-assisted MIMO link is tackled in [42], considering that the RIS is deployed to assist the communication between the transmitter and the receiver. In [43], the problem of power control for physical-layer broadcasting under quality of service constraints for the mobile users is addressed in RIS-empowered networks. The downlink of a MIMO multi-cell system is considered in [44], where an RIS is deployed at the boundary between multiple cells. Therein, the problem of weighted sum-rate maximization is tackled by alternating optimization of the base station beamformer and of the RIS phase shifts. RIS-based mmWave systems are considered in [45], with reference to a single-user MISO channel. The transmit beamforming and the RIS phase shifts are optimized considering both the single-RIS and multi-RIS cases. In [46], the problem of joint channel estimation and sum-rate maximization is tackled in the uplink of a single-user RIS-based system, where the phase shifts of the RIS have a discrete resolution.

B. Novelty and Contribution

The common denominator of all the above works dealing with radio resource allocation is that the optimization is focused only on the data communication phase, whereas the overhead required to estimate the channel state information and to report the optimized phase shifts configuration to the RIS is not taken into account. As recently highlighted in [10], the overhead for resource

allocation in RIS-empowered wireless networks may be more critical than in conventional wireless networks, due to the possibly large number of unit-cells in each RIS that may be spatially distributed throughout the network. Moreover, all above works propose solutions for the allocation of the phase shifts of the RISs that are obtained by using numerical methods, which makes it difficult to assess the ultimate performance of RIS-empowered wireless networks.

In contrast, this work develops a resource allocation framework that explicitly accounts for the overhead associated with channel estimation and with the configuration of the optimal RIS phase shifts. A point-to-point RIS-based system is considered, with multiple antennas at the transmitter and receiver. More precisely, the following specific contributions are made:

- We propose a model to account for channel estimation and for the overhead required for the configuration of the RIS phase shifts. Based on the overhead-aware expressions of the system rate and energy efficiency, we develop efficient radio resource allocation algorithms.
- We derive two methods for the joint optimization of the RIS phase shifts, and of the transmit and receive filters. Both methods are expressed in closed-form, thus requiring a negligible computational complexity compared to state-of-the-art methods based on alternating optimization, as well as enabling analytical performance evaluation of RIS-empowered wireless networks. Both approaches are provably optimal in the case of rank-one channels, which includes the notable special case of single-antenna transmitters and receivers.
- We introduce globally optimal algorithms for computing the power and bandwidth that maximize the rate, the energy efficiency, and their trade-off. This is shown to involve only convex/pseudo-convex problems, which have affordable complexity.
- Finally, we provide extensive numerical results to show the performance of the proposed approaches. We find that our proposed closed-form phase allocations perform similar to more complex, state-of-the-art numerical methods, e.g. alternating optimization approaches.

The rest of the paper is organized as follows. Section II introduces the system model and the problem statement. Section III develops the optimization methods for the allocation of the RIS phase shifts, the transmit beamforming vector, and the receive filter. Section IV addresses the optimization of the powers and bandwidths for the maximization of the system rate, energy efficiency, and the derivation of the optimal rate-energy trade-off. Section V numerically analyzes the proposed optimization methods. Finally, concluding remarks are given in Section VI.

II. SYSTEM MODEL AND PROBLEM STATEMENT

We consider a point-to-point system where a transmitter equipped with N_T antennas and a receiver equipped with N_R antennas communicate through an RIS. We denote by \mathbf{H} and \mathbf{G} the channels from the transmitter to the RIS and from the RIS to the receiver, respectively, by \mathbf{q} the unit-norm transmit beamformer, and by \mathbf{w} the unit-norm receive combiner. We assume that no direct link between the transmitter and receiver exists. According to [15] and [16], we assume that the RIS is made of N elementary unit-cells, which are capable of independently reflecting the radio wave impinging upon them, applying a phase shift denoted by ϕ_n , with $n = 1, \dots, N$. We collect all RIS phase shifts in the diagonal matrix $\mathbf{\Phi} = \text{diag}(e^{j\phi_1}, \dots, e^{j\phi_N})$.

Before the data transmission phase starts, it is required to estimate the channels \mathbf{H} and \mathbf{G} , and configure the optimized phase shifts at the RIS. More details on channel estimation and RIS phase shifts configuration is provided in Section III-D. Nevertheless, at this stage it is important to stress that both channel estimation and resource optimization can be performed either at the transmitter or at the receiver, but not at the RIS, since the RIS is not capable of any signal processing operation. This poses the problem of feeding back the optimized phase matrix $\mathbf{\Phi}$ to the RIS before the data transmission phase can start, which may introduce a non-negligible overhead to the communication phase, especially for large N . Let us denote by T_F the duration of the feedback phase, which will depend on the power p_F used during the feedback phase and on the bandwidth B_F of the feedback channel. Moreover, let us denote by T_E the duration of the channel estimation phase prior to feedback and communication. Mathematical expressions of T_F and T_E are provided in Section III-D.

Denoting by T the total duration of the time slot comprising channel estimation, feedback, and data communication, the system achievable rate can be expressed as

$$R(p, B, p_F, B_F, \mathbf{\Phi}, \mathbf{q}, \mathbf{w}) = \left(1 - \frac{T_E + T_F}{T}\right) B \log \left(1 + \frac{p |\mathbf{w}^H \mathbf{G} \mathbf{\Phi} \mathbf{H} \mathbf{q}|^2}{BN_0}\right), \quad (1)$$

while the system energy efficiency is written as

$$\text{EE}(p, B, p_F, B_F, \mathbf{\Phi}, \mathbf{q}, \mathbf{w}) = \frac{R(p, B, p_F, B_F, \mathbf{\Phi}, \mathbf{q}, \mathbf{w})}{P_{tot}(p, B, p_F, B_F)}, \quad (2)$$

wherein P_{tot} denotes the total power consumption in the whole timeframe T , which is equal to

$$P_{tot}(p, B, p_F, B_F) = P_E + \frac{1}{T} [(T - T_E - T_F)\mu p + \mu_F p_F T_F + T P_c], \quad (3)$$

since a power p is used for $T - T_E - T_F$ seconds, with transmit amplifier efficiency $1/\mu$, a power p_F for T_F seconds, with transmit amplifier efficiency $1/\mu_F$, while hardware static power consumption takes place for the whole interval T , where P_c denotes the static hardware power required to operate the RIS and any other system component, and P_E accounts for the energy consumption for channel estimation, which is further detailed in Section III-D.

Unlike previous studies, this work jointly optimizes the transmit and feedback powers and bandwidths p, p_F, B, B_F , the RIS matrix Φ , and the transmit and receive filters \mathbf{q}, \mathbf{w} , in order to maximize the rate (1), the energy efficiency (2), and derive the system rate-energy Pareto-region.

III. OPTIMIZATION OF $\Phi, \mathbf{q}, \mathbf{w}$

As a first step, let us fix the variables p, p_F, B, B_F , and focus on optimizing the RIS phase shift matrix Φ , the unit-norm beamforming vector \mathbf{q} , and the unit-norm linear receive filter \mathbf{w} . It can be seen that the variable $\Phi, \mathbf{q}, \mathbf{w}$ do not appear in the denominator of the energy efficiency, but only in the numerator, which coincides with the system sum-rate. Thus, with respect to $\Phi, \mathbf{q}, \mathbf{w}$, both the rate and energy efficiency are maximized by solving the problem

$$\max_{\Phi, \mathbf{q}, \mathbf{w}} |\mathbf{w}^H \mathbf{G} \Phi \mathbf{H} \mathbf{q}|^2 \quad (4a)$$

$$\text{s.t. } \|\mathbf{q}\| = \|\mathbf{w}\| = 1, 0 \leq \phi_n \leq 2\pi, \forall n = 1, \dots, N. \quad (4b)$$

Problem (4) is challenging because the objective contains a product of three variables, among which one, the RIS phase shift matrix, is diagonal with unit-modulus components. It is known that, denoting by $\lambda_{A, \max}$ the largest singular value of \mathbf{A} , it holds that

$$\max_{(\mathbf{w}, \mathbf{q}) : \|\mathbf{w}\| = \|\mathbf{q}\| = 1} |\mathbf{w}^H \mathbf{A} \mathbf{q}|^2 \leq \max_{(\mathbf{w}, \mathbf{q}) : \|\mathbf{w}\| = \|\mathbf{q}\| = 1} \|\mathbf{w}\|^2 \|\mathbf{A} \mathbf{q}\|^2 \leq \max_{\mathbf{q} : \|\mathbf{q}\| = 1} \|\mathbf{A} \mathbf{q}\|^2 = \lambda_{A, \max}^2, \quad (5)$$

where we have used Cauchy-Schwarz inequality, the constraint that $\|\mathbf{w}\| = 1$, and the fact that the maximum of $\|\mathbf{A} \mathbf{q}\|$ with respect to the set of unit-norm vectors \mathbf{q} is the spectral norm of \mathbf{A} , i.e. the largest singular value of \mathbf{A} , [47, pag. 148]. Then, for any \mathbf{A} , the optimal \mathbf{q} and \mathbf{w} are the dominant right and left eigenvector of the \mathbf{A} , since this achieves the upper-bound in (5). However, at this point one should maximize the largest singular value of $\mathbf{A} = \mathbf{G} \Phi \mathbf{H}$ with respect to Φ , which is prohibitive to be performed optimally, due to the involved relationship between the singular values of $\mathbf{G} \Phi \mathbf{H}$ and the matrix Φ . Furthermore, this would not yield any

closed-form (even approximate) expression of Φ , \mathbf{q} , \mathbf{w} , which hinders the analytical evaluation of the ultimate performance of RISs in wireless networks.

In the following we propose two closed-form approaches to tackle (4), which optimize either an upper-bound or a lower-bound of (4a). Moreover, for benchmarking purposes, we also consider a third method based on the use of alternating maximization, that is the typical approach in previous literature, but that has higher complexity, without providing a closed-form solution.

A. Optimizing an upper-bound of (4a)

Let $\mathbf{H} = \sum_{j=1}^{r_H} \mu_{j,H} \mathbf{u}_{j,H} \mathbf{v}_{j,H}^H$ and $\mathbf{G} = \sum_{i=1}^{r_G} \mu_{i,G} \mathbf{u}_{i,G} \mathbf{v}_{i,G}^H$ be the singular value decompositions of \mathbf{H} and \mathbf{G} , with $r_H = \text{rank}(\mathbf{H})$ and $r_G = \text{rank}(\mathbf{G})$. Then, (4a) is upper-bounded as

$$|\mathbf{w}^H \mathbf{G} \Phi \mathbf{H} \mathbf{q}|^2 = \left| \sum_{i=1}^{r_G} \sum_{j=1}^{r_H} \mu_{i,G} \mu_{j,H} \mathbf{w}^H \mathbf{u}_{i,G} \mathbf{v}_{i,G}^H \Phi \mathbf{u}_{j,H} \mathbf{v}_{j,H}^H \mathbf{q} \right|^2 \stackrel{(a)}{\leq} \left(\sum_{i=1}^{r_G} \sum_{j=1}^{r_H} \mu_{i,G} \mu_{j,H} |\mathbf{w}^H \mathbf{u}_{i,G}| |\mathbf{v}_{i,G}^H \Phi \mathbf{u}_{j,H}| |\mathbf{v}_{j,H}^H \mathbf{q}| \right)^2 \stackrel{(b)}{\leq} r_G r_H \sum_{i=1}^{r_G} \sum_{j=1}^{r_H} \mu_{i,G}^2 \mu_{j,H}^2 |\mathbf{w}^H \mathbf{u}_{i,G}|^2 |\mathbf{v}_{i,G}^H \Phi \mathbf{u}_{j,H}|^2 |\mathbf{v}_{j,H}^H \mathbf{q}|^2 \quad (6)$$

wherein Inequality (a) is due to the triangle inequality, while Inequality (b) is a special case of Cauchy-Schwarz inequality.¹ In the following, we derive a closed-form solution for the maximization of the bound in (6) with respect to Φ , \mathbf{w} , \mathbf{q} . We start with the following lemma.

Lemma 1: Consider $c_j \geq 0$ and $x_j \geq 0$ for all $j = 1, \dots, J$, with $\sum_{j=1}^J x_j \leq 1$. Then it holds that $\max \sum_{j=1}^J c_j x_j \leq c_{\bar{j}}$, with \bar{j} such that $c_{\bar{j}} \geq c_j$ for all $j = 1, \dots, J$.

Proof: Since $c_{\bar{j}} \geq c_j$ for all $j = 1, \dots, J$, there exist non-negative $\epsilon_1, \dots, \epsilon_J$ such that $c_j = c_{\bar{j}} - \epsilon_j$, for all $j = 1, \dots, J$. Then, the result is shown as follows

$$\sum_{j=1}^J c_j x_j = c_{\bar{j}} \sum_{j=1}^J x_j - \sum_{j \neq \bar{j}} \epsilon_j x_j \leq c_{\bar{j}} \sum_{j=1}^J x_j - \sum_{j=2}^J \epsilon_j x_j \leq c_{\bar{j}} \sum_{j=1}^J x_j \leq c_{\bar{j}}. \quad (7)$$

■

At this point, we are ready to derive the optimal Φ , \mathbf{q} , and \mathbf{w} for the upper-bound in (6).

Proposition 1: For any p, B, p_F, B_F , defining

$$\bar{j}(i) = \underset{j}{\text{argmax}} \mu_{j,H}^2 \left(\sum_{n=1}^N \left| \mathbf{v}_{i,G}^{(n)} \right| \left| \mathbf{u}_{j,H}^{(n)} \right| \right)^2, \forall i = 1, \dots, r_G, \quad \bar{i} = \underset{i}{\text{argmax}} \mu_{i,G}^2 \mu_{\bar{j}(i),H}^2 \left(\sum_{n=1}^N \left| \mathbf{v}_{i,G}^{(n)} \right| \left| \mathbf{u}_{\bar{j}(i),H}^{(n)} \right| \right)^2 \quad (8)$$

¹Cauchy-Schwarz inequality states that $(\sum_{m=1}^M a_m b_m)^2 \leq (\sum_{m=1}^M a_m^2)(\sum_{m=1}^M b_m^2)$, for any non-negative numbers $\{a_m, b_m\}_{m=1}^M$. Then, by taking $b_m = 1$ for all m , we obtain $(\sum_{m=1}^M a_m)^2 \leq M \sum_{m=1}^M a_m^2$

the global maximizer of the upper-bound in (6) is obtained by setting the beamforming vector as $\mathbf{q} = \mathbf{v}_{\bar{j}(\bar{i}),H}$, the receive filter as $\mathbf{w} = \mathbf{u}_{\bar{i},G}$, and the RIS phase shifts are $\phi_n = -\angle \left\{ \mathbf{v}_{\bar{i},G}^{*(n)} \mathbf{u}_{\bar{j}(\bar{i}),H}^{(n)} \right\}$, with $(*)$ denoting complex conjugate.

Proof: In order to maximize the upper-bound in (6), we can neglect the constant multiplicative term $r_G r_H$, and we observe that

$$\begin{aligned} & \sum_{i=1}^{r_G} \sum_{j=1}^{r_H} \mu_{i,G}^2 \mu_{j,H}^2 |\mathbf{w}^H \mathbf{u}_{i,G}|^2 |\mathbf{v}_{i,G}^H \Phi \mathbf{u}_{j,H}|^2 |\mathbf{v}_{j,H}^H \mathbf{q}|^2 \\ & \leq \sum_{i=1}^{r_G} \mu_{i,G}^2 |\mathbf{w}^H \mathbf{u}_{i,G}|^2 \underbrace{\sum_{j=1}^{r_H} \mu_{j,H}^2 \max_{\Phi} \{ |\mathbf{v}_{i,G}^H \Phi \mathbf{u}_{j,H}|^2 \}}_{y_i} |\mathbf{v}_{j,H}^H \mathbf{q}|^2. \end{aligned} \quad (9)$$

wherein the inequality follows upon taking the maximum over Φ . Next, for any $i = 1, \dots, r_G$, the term y_i defined in the last line of (9) can be upper-bounded as

$$\begin{aligned} y_i &= \sum_{j=1}^{r_H} \mu_{j,H}^2 \max_{\Phi} \{ |\mathbf{v}_{i,G}^H \Phi \mathbf{u}_{j,H}|^2 \} |\mathbf{v}_{j,H}^H \mathbf{q}|^2 \stackrel{(a)}{\leq} \\ & \mu_{\bar{j}(\bar{i}),H}^2 \max_{\Phi} \{ |\mathbf{v}_{i,G}^H \Phi \mathbf{u}_{\bar{j}(\bar{i}),H}|^2 \} \stackrel{(b)}{=} \mu_{\bar{j}(\bar{i}),H}^2 \left(\sum_{n=1}^N \left| \mathbf{v}_{i,G}^{(n)} \right| \left| \mathbf{u}_{\bar{j}(\bar{i}),H}^{(n)} \right| \right)^2, \end{aligned} \quad (10)$$

wherein (b) follows because, for any $i = 1, \dots, r_G$, the optimal Φ is the one that compensates the phase shifts between the components of $\mathbf{v}_{i,G}^H$ and of $\mathbf{u}_{\bar{j}(\bar{i}),H}$, while (a) follows from Lemma 1 since $\sum_{j=1}^{r_H} |\mathbf{v}_{j,H}^H \mathbf{q}|^2 \leq \|\mathbf{q}\|^2 = 1$, since, for all $j = 1, \dots, r_H$, $\mathbf{v}_{j,H}^H \mathbf{q}$ is the projection of the unit-norm vector \mathbf{q} onto the orthonormal vector $\mathbf{v}_{j,H}$. Then, plugging (10) into (9), yields

$$|\mathbf{w}^H \mathbf{G} \Phi \mathbf{H} \mathbf{q}|^2 \leq \sum_{i=1}^{r_G} \mu_{i,G}^2 \mu_{\bar{j}(\bar{i}),H}^2 \left(\sum_{n=1}^N \left| \mathbf{v}_{i,G}^{(n)} \right| \left| \mathbf{u}_{\bar{j}(\bar{i}),H}^{(n)} \right| \right)^2 |\mathbf{w}^H \mathbf{u}_{i,G}|^2 \leq \mu_{\bar{i},G}^2 \mu_{\bar{j}(\bar{i}),H}^2 \left(\sum_{n=1}^N \left| \mathbf{v}_{\bar{i},G}^{(n)} \right| \left| \mathbf{u}_{\bar{j}(\bar{i}),H}^{(n)} \right| \right)^2$$

wherein the last inequality holds again by Lemma 1. Finally, the result follows since all inequalities in this proof hold with equality upon choosing $\Phi, \mathbf{q}, \mathbf{w}$ as in the thesis of the proposition. \blacksquare

Remark 1: The bound in (6) is tight when $r_G = r_H = 1$. Then, the approach developed in this section is optimal for Problem (4) when the channels to and from the RIS have unit-rank (e.g. when transmitter and receiver have a single antenna).

B. Optimizing a lower-bound of (4a)

Define $\mathbf{g}_w = \mathbf{G}^H \mathbf{w}$, $\mathbf{h}_q = \mathbf{H} \mathbf{q}$, and observe that, for any fixed \mathbf{q} and \mathbf{w} , the optimal Φ for Problem (4) is such that $\phi_n = -\angle\{\mathbf{g}_w^*(n)\mathbf{h}_q(n)\}$, for all $n = 1, \dots, N$. Next, denoting by $\mathbf{h}_n^T \in \mathcal{R}^{1 \times N}$ and $\mathbf{g}_n \in \mathcal{R}^{N \times 1}$ the n -th row of \mathbf{H} and the n -th column of \mathbf{G} , respectively, with $n = 1, \dots, N$, it holds that $\mathbf{g}_w(n) = \mathbf{w}^H \mathbf{g}_n$ and $\mathbf{h}_q(n) = \mathbf{h}_n^T \mathbf{q}$. Then, it holds that

$$\max_{\mathbf{q}, \mathbf{w}, \Phi} |\mathbf{w}^H \mathbf{G} \Phi \mathbf{H} \mathbf{q}|^2 = \max_{\mathbf{q}, \mathbf{w}} \left(\max_{\Phi} |\mathbf{g}_w^H \Phi \mathbf{h}_q|^2 \right) \stackrel{(a)}{=} \max_{\mathbf{q}, \mathbf{w}} \left(\sum_{n=1}^N |\mathbf{w}^H \mathbf{g}_n \mathbf{h}_n^T \mathbf{q}| \right)^2 \stackrel{(b)}{\geq} \max_{\mathbf{q}, \mathbf{w}} \left| \mathbf{w}^H \left(\sum_{n=1}^N \mathbf{g}_n \mathbf{h}_n^T \right) \mathbf{q} \right|^2 \quad (11)$$

where Equality (a) holds plugging in the maximizer with respect to Φ , i.e. $\phi_n = -\angle\{\mathbf{g}_w^*(n)\mathbf{h}_q(n)\}$, while Inequality (b) holds due to the triangle inequality. Then, following a similar argument as the one used to obtain (5), the last maximization in (11) is solved by choosing \mathbf{q}, \mathbf{w} as the dominant right and left eigenvector of the matrix $\sum_{n=1}^N \mathbf{g}_n \mathbf{h}_n^T$.

C. Tackling (4) by alternating maximization

As a benchmark solution, let us maximize $|\mathbf{w}^H \mathbf{G} \Phi \mathbf{H} \mathbf{q}|^2$ by alternatively optimizing Φ , for fixed \mathbf{w}, \mathbf{q} , and then \mathbf{w}, \mathbf{q} , for fixed Φ . To solve these two subproblems, we observe that, for fixed Φ , the optimal \mathbf{w} and \mathbf{q} are derived as the dominant left and right eigenvectors of the matrix $\mathbf{A} = \mathbf{G} \Phi \mathbf{H}$, as shown in (5). On the other hand, for fixed \mathbf{w} and \mathbf{q} , the problem is reduced to maximizing the term $\mathbf{g}_w^H \Phi \mathbf{h}_q$ with $\mathbf{g}_w = \mathbf{G}^H \mathbf{w}$ and $\mathbf{h}_q = \mathbf{H} \mathbf{q}$, whose maximization is obtained when Φ is such that $\phi_n = -\angle\{\mathbf{g}_w^*(n)\mathbf{h}_q(n)\}$, for all $n = 1, \dots, N$, as discussed in Section III-B. Thus, an alternating maximization algorithm can be formally stated as in Algorithm 1.

Algorithm 1 Alternating optimization of $\Phi, \mathbf{q}, \mathbf{w}$

Initialize \mathbf{w} and \mathbf{q} to feasible values.

repeat

$\mathbf{g}_w = \mathbf{G}^H \mathbf{w}$ and $\mathbf{h}_q = \mathbf{H} \mathbf{q}$; set $\phi_n = -\angle\{\mathbf{g}_w^*(n)\mathbf{h}_q(n)\}$ for all $n = 1, \dots, N$;

$\mathbf{A} = \mathbf{G} \Phi \mathbf{H}$; set \mathbf{w} as the left dominant eigenvector of \mathbf{A} and \mathbf{q} as the right dominant eigenvector of \mathbf{A} ;

until Convergence

D. Overhead modeling

In this section, the necessary details about the channel estimation and feedback phases are provided and a mathematical expression for T_F , T_E , and P_E will be derived. For the sake

of argument, and without loss of generality, we assume that channel estimation and resource optimization takes place at the transmitter.²

As for T_F , after resource optimization, the transmitter sends a control signal to the RIS to configure the phase shifts.³ Denoting by h_F the scalar feedback channel from the RIS to the transmitter, it holds that $T_F = \frac{Nb_F}{B_F \log\left(1 + \frac{p_F |h_F|^2}{N_0 B_F}\right)}$, with b_F the number of feedback bits for each unit-cell of the RIS and N_0 the noise power spectral density. As anticipated, T_F depends on p_F and B_F , which complicates the mathematical structure of the rate in (1) and of the energy efficiency in (2), making the optimization of these two metrics, and of their trade-off, with respect to p, p_F, B, B_F , challenging to tackle. The optimization of p, p_F, B, B_F for the maximization of the rate, the energy efficiency, and their trade-off is addressed in Section IV.

As for T_E , we assume a time division duplex (TDD) protocol in which the receiver sends pilot signals to the transmitter, through the RIS, which, in this phase, does not apply any phase shift, i.e. $\phi_n = 0$ for all $n = 1, \dots, N$, [48]. Thus, the $NN_T N_R$ product channels $h_{nt,n} g_{n,nr}$ are estimated, with $h_{nt,n}$ denoting the channel from the nt -th transmit antenna to the n -th RIS elements, and $g_{n,nr}$ denoting the channel from the n -th RIS element to the nr -th receive antenna. Moreover, one additional pilot tone is required for the transmitter to estimate the feedback channel. Therefore, denoting by T_0 the duration of each pilot tone, it holds $T_E = (N_T N N_R + 1)T_0$. It should be remarked that the knowledge of the product channels $h_{nt,n} g_{n,nr}$ is enough to reconstruct the matrix \mathbf{A} in (5) and, therefore, to optimally solve (4) with respect to the phase shifts of the RIS, the beamforming vector, and the receive filter. For generality, the overhead needed for channel estimation is estimated based on the channel state information needed to optimally solve (4). However, our algorithms could be applied based on any practical channel estimation algorithms that was recently reported in the literature, e.g., [48]. Moreover, based on the expressions of T_F and T_E , the power consumption in (3) becomes

$$P_{tot} = P_E + \frac{b_F N (\mu_F p_F - \mu p)}{T B_F \log\left(1 + \frac{p_F |h_F|^2}{B_F N_0}\right)} + \mu p \left(1 - \frac{T_E}{T}\right) + P_c, \quad (12)$$

where $P_E = P_0(1 + NN_T N_R)$ accounts for the energy consumption for channel estimation, and P_0 denotes the power of each pilot tone.

²A similar argument would hold in the case in which channel estimation and resource optimization took place at the receiver.

³Here we neglect the feedback of the receive filter \mathbf{w} to the receiver, because, first it is negligible with respect to the feedback of the RIS phase shifts, since typically $N \gg N_R$, and, second, because the focus of this work is on the RIS and on evaluating the feedback required to operate it.

IV. OPTIMIZATION OF p, p_F, B, B_F .

After optimizing $\Phi, \mathbf{q}, \mathbf{w}$ by any of the methods developed in Section III, we are left with the problem of optimizing the transmit powers p, p_F , and the bandwidths B, B_F . It should be stressed that, as already mentioned, the optimized $\Phi, \mathbf{q}, \mathbf{w}$ that are obtained from any of the algorithms developed in Section III, do not depend on any of the variables p, p_F, B, B_F , but only on the channels \mathbf{H} and \mathbf{G} . Moreover, as already mentioned, the optimized $\Phi, \mathbf{q}, \mathbf{w}$ are the same for both the rate and the energy efficiency. Thus, it is possible to simply plug in the optimized $\Phi, \mathbf{q}, \mathbf{w}$ into the objective to maximize, thus effectively decoupling the optimization of p, p_F, B, B_F from the optimization of $\Phi, \mathbf{q}, \mathbf{w}$.

On the other hand, unlike the optimization of $\Phi, \mathbf{q}, \mathbf{w}$, the optimization of p, p_F, B, B_F depends on whether the objective function is the rate or the energy efficiency, or whether their optimal trade-off is to be optimized. Therefore, these problems will be treated separately.

A. Rate maximization

The rate maximization problem is stated as the following optimization program

$$\max_{p, B, p_F, B_F} R(p, B, p_F, B_F, \Phi_{\text{opt}}, \mathbf{q}_{\text{opt}}, \mathbf{w}_{\text{opt}}) \quad (13a)$$

$$\text{s.t. } p + p_F \leq P_{\max}, B + B_F \leq B_{\max} \quad (13b)$$

$$p \geq 0, p_F \geq 0, B \geq 0, B_F \geq 0 \quad (13c)$$

$$\frac{b_F N}{TB_F \log\left(1 + \frac{p_F |h_F|^2}{B_F N_0}\right)} \leq 1 - \frac{T_E}{T}, \quad (13d)$$

In order to solve Problem (13) let us first explicitly write its objective function (1) as a function of the optimization variables p, p_F, B, B_F

$$R(p, B, p_F, B_F) = \left(\beta - \frac{d}{B_F \log\left(1 + \frac{p_F |h_F|^2}{N_0 B_F}\right)} \right) B \log\left(1 + \frac{p |\mathbf{w}_{\text{opt}}^H \mathbf{G} \Phi_{\text{opt}} \mathbf{H} \mathbf{q}_{\text{opt}}|^2}{B N_0}\right), \quad (14)$$

wherein $\beta = 1 - T_E/T$ and $d = b_F N/T$. Thus, being the product of two functions, the objective of (13) is not jointly concave in all optimization variables, which makes Problem (13) challenging to solve with affordable complexity. Indeed, the product of functions is in general not concave even in the simple case in which the individual factors are concave. Moreover, in the case at hand, the concavity of the two factors defining (14) is not clear, either. Thus, in order to solve

$$\mathcal{H} = \frac{1}{(B_F + ap_F)^2 z^3(p_F, B_F)} \times \quad (17)$$

$$\begin{bmatrix} a^2 B_F z(p_F, B_F) + 2a^2 B_F^2 & -a^2 p_F z(p_F, B_F) + 2a B_F (B_F + ap_F) z'_{B_F}(p_F, B_F) \\ -a^2 p_F z(p_F, B_F) + 2a B_F (B_F + ap_F) z'_{B_F}(p_F, B_F) & \frac{a^2 p_F^2}{B_F} z(p_F, B_F) + 2(B_F + ap_F)^2 \left(z'_{B_F}(p_F, B_F) \right)^2 \end{bmatrix}$$

(13), it is not possible to directly use standard convex optimization algorithms. In the rest of this section we show that it is possible to reformulate Problem (13) into a convex optimization problem without any loss of optimality. To this end, some preliminary lemmas are needed.

Lemma 2: The function $R(p, B, p_F, B_F)$ is jointly increasing and jointly concave in (p, B) .

Proof: Neglecting inessential constant terms (with respect to p and B), and defining

$$c = \frac{|\mathbf{w}_{\text{opt}}^H \mathbf{G} \Phi_{\text{opt}} \mathbf{H} \mathbf{q}_{\text{opt}}|^2}{N_0}, \quad (15)$$

Eq. (13a) is equivalent to the function $g_1(p, B) = B \log\left(1 + \frac{pc}{B}\right)$, which can be seen to be the perspective of the concave function $\log(1 + pc)$ [49]. Thus, since the perspective operator preserves concavity, g_1 is jointly concave in (p, B) . Moreover, g_1 is clearly increasing in p , while inspecting the derivative of g_1 with respect to B , and exploiting that $(1 + y) \log(1 + y) \geq y$ for any $y \geq 0$, shows that g_1 is increasing in B . ■

Lemma 3: The function $R(p, B, p_F, B_F)$ is jointly increasing and jointly concave in (p_F, B_F) .

Proof: Neglecting inessential constant terms (with respect to p_F and B_F), it can be seen that, upon defining $a = |h_F|^2/N_0$, the function in (13a) is equivalent to the function

$$\beta - \frac{d}{B_F \log\left(1 + a \frac{p_F}{B_F}\right)}. \quad (16)$$

Showing the joint concavity of (16) with respect to (p_F, B_F) is equivalent to showing that the function $g_2(p_F, B_F) = \frac{1}{B_F \log\left(1 + a \frac{p_F}{B_F}\right)} = \frac{1}{z(p_F, B_F)}$, is jointly convex in (p_F, B_F) . After some elaborations the Hessian matrix of g_2 is written as in (17), shown at the top of this page, wherein $z'_{B_F}(p_F, B_F) = \log\left(1 + a \frac{p_F}{B_F}\right) - \frac{ap_F}{B_F + ap_F}$ is the first-order derivative of z with respect to B_F . Clearly, the entry (1, 1) of \mathcal{H} is non-negative. Thus, \mathcal{H} is positive semi-definite if its determinant is non-negative, too. Then, since the second derivative of z with respect to B_F can be written as

$$z''_{B_F}(p_F, B_F) = -\frac{ap_F^2}{B_F (B_F + ap_F)^2}, \quad (18)$$

after some elaborations, the non-negativity of the Hessian of \mathcal{H} leads to the condition $(B_F + ap_F)^2(z'(p_F, B_F))^2 + 2a^2p_F^2 + 2ap_Fz'(p_F, B_F) \geq 0$, which holds if $z'(p_F, B_F)$ is non-negative, which is true by virtue of the inequality $(1 + y) \log(1 + y) \geq y$. Moreover, the non-negativity of $z'(p_F, B_F)$ implies that $z(p_F, B_F)$ is increasing in B_F , while the fact that it is increasing in p_F is apparent. ■

Leveraging Lemmas 2 and 3, it is possible to equivalently reformulate Problem (13) into a convex problem, which can then be efficiently solved by means of any convex optimization method. To this end, the first step is to observe that taking the logarithm of the objective in (13a) does not change the optimal solutions of (13a), since the logarithm is an increasing function. Then, an equivalent reformulation of (13a) is the following problem

$$\max_{p, B, p_F, B_F} \log(\beta - dg_2(p_F, B_F)) + \log(g_1(p, B)) \quad (19a)$$

$$\text{s.t. } p + p_F \leq P_{max}; B + B_F \leq B_{max} \quad (19b)$$

$$p \geq 0, p_F \geq 0; B \geq 0, B_F \geq 0 \quad (19c)$$

$$\frac{d}{B_F \log\left(1 + \frac{p_F |h_F|^2}{B_F N_0}\right)} \leq \beta, \quad (19d)$$

which is a convex optimization problem by virtue of Lemmas 2 and 3. Indeed, (19a) is a concave function since Lemmas 2 and 3 ensure that both summands are concave. Also, all the constraints in (19b)-(19c) are linear, while (19d) is convex thanks to Lemma 3. Thus, Problem (19) is a convex problem that has the same set of solutions as Problem (13), with the advantage that it can be conveniently solved by using standard convex optimization algorithms.

Finally, in order to further simplify the solution of (19), we observe that the optimal solution of (19) is such that (19b) and (19c) must be fulfilled with equality, since the objective function is increasing in all arguments and (19d) is decreasing in both B_F and p_F . Thus, Problem (19) can be reformulated, without loss of optimality, as

$$\max_{p, B} \log(\beta - dg_2(P_{max} - p, B_{max} - B)) + \log(g_1(p, B)) \quad (20a)$$

$$\text{s.t. } 0 \leq p \leq P_{max}, 0 \leq B \leq B_{max}, \frac{d}{(B_{max} - B) \log\left(1 + \frac{(P_{max} - p) |h_F|^2}{(B_{max} - B) N_0}\right)} \leq \beta, \quad (20b)$$

which has only two optimization variables. Upon solving (20), the optimal feedback power and bandwidth are retrieved as $p_F = P_{max} - p$ and $B_F = B_{max} - B$. Problem (20) is clearly still

$$\frac{da}{(B_F + a(P_{max} - p)) \left(\beta B_F \log \left(1 + a \frac{(P_{max} - p)}{B_F} \right) - d \right) \left(\log \left(1 + (P_{max} - p) \frac{a}{B_F} \right) \right)}$$

$$= \frac{c}{(B + pc) \log \left(1 + \frac{pc}{B} \right)} \quad (23)$$

a convex problem, since it is obtained from the convex Problem (19) upon applying the linear variable transformations $p_F = P_{max} - p$ and $B_F = B_{max} - B$, and linear transformations are well-known to preserve convexity.

Finally, after developing a method for solving (20) with affordable complexity, in the last part of this section we focus on obtaining closed-form solutions for the special cases of Problem (20) obtained by considering the optimization of the transmit powers for fixed bandwidths and vice-versa. Then closed-form solutions can be obtained as shown in the next two subsections.

1) *Optimization for fixed B and B_F*: Assume that B and B_F are fixed in Problem (20). Then, Problem (20) reduces to

$$\max_p \log(\beta - dg_2(P_{max} - p, B_F)) + \log(g_1(p, B)) \quad (21a)$$

$$\text{s.t. } 0 \leq p \leq P_{max} - \frac{B_F N_0}{|h_F|^2} \left(e^{\frac{d}{B_F \beta}} - 1 \right) . \quad (21b)$$

Proposition 2: Let \bar{p} be the unique stationary point of (21a). Then, Problem (21) has a unique solution given by

$$p^* = \min(\bar{p}, P_{max} - p_{min}) , \quad (22)$$

Proof: Equating the first-order derivative of (21a) to zero yields the stationarity equation in (23), shown at the top of this page. The above equation can be seen to have always a solution, since the left-hand-side is decreasing in p and tending to ∞ for $p \rightarrow 0^+$, while the right-hand-side is increasing in p , taking a finite value for $p = 0$ and tending to ∞ for $p \rightarrow P_{max}$. Then, (21a) has a unique solution \bar{p} , since (21a) is a strictly concave function of p , as it is the sum of concave functions and $\log(g_1(p, B))$ is strictly concave in p . Finally, (23) also shows that (21a) is strictly increasing for $p < \bar{p}$ and strictly decreasing for $p > \bar{p}$.

Thus, we can conclude that the unique solution of Problem (21) is either \bar{p} , if $\bar{p} \leq P_{max}$, or it is P_{max} itself, which yields (22). ■

$$\frac{\log\left(1 + \frac{cp}{B}\right) - \frac{cp}{B+cp}}{B \log\left(1 + \frac{cp}{B}\right)} = \frac{\left(\log\left(1 + \frac{ap_F}{B_{max}-B}\right) - \frac{ap_F}{B_{max}-B+ap_F}\right) d}{\left(\beta(B_{max}-B) \log\left(1 + \frac{ap_F}{B_{max}-B}\right) - d\right) (B_{max}-B) \log\left(1 + \frac{ap_F}{B_{max}-B}\right)} \quad (27)$$

Finally, the optimal feedback power is obtained as $p_F^* = P_{max} - p^*$.

2) *Optimization for fixed p and p_F* : Assume that p and p_F are fixed in Problem (20). Then, Problem (20) reduces to

$$\max_{B, B_F} \log(\beta - dg_2(B_{max} - B, p_F)) + \log(g_1(p, B)) \quad (24a)$$

$$\text{s.t. } 0 \leq B \leq B_{max} - \hat{B}, \quad (24b)$$

with \hat{B} the unique⁴ solution of the equation

$$(B_{max} - B) \log\left(1 + \frac{p_F |h_F|^2}{N_0(B_{max} - B)}\right) \geq \frac{d}{\beta}. \quad (25)$$

Proposition 3: Problem (24) has a unique solution given by

$$B^* = \min(\bar{B}, B_{max} - \hat{B}), \quad (26)$$

with \bar{B} the unique stationary point of (24a).

Proof: The proof follows along the same lines as for Proposition 2. The objective (24a) is strictly concave, has a unique stationary point \bar{B} , which is given by the solution of the stationarity equation in (27), shown above, and is strictly increasing for $B < \bar{B}$ and strictly decreasing for $\bar{B} > B$. ■

Finally, the optimal feedback bandwidth is obtained as $B_F^* = B_{max} - B^*$.

B. Energy efficiency optimization

As for the optimization of the energy efficiency, plugging again any of the allocations of $\Phi, \mathbf{q}, \mathbf{w}$ developed in Section III into the energy efficiency function, leads us to the following

⁴The solution is unique because the function at the LHS is strictly decreasing, as it immediately follows from previous results.

problem to solve

$$\max_{p, B, p_F, B_F} \frac{R(p, B, p_F, B_F, \Phi^{\text{opt}}, \mathbf{q}^{\text{opt}}, \mathbf{w}^{\text{opt}})}{P_{\text{tot}}(p, p_F, B_F)} \quad (28a)$$

$$\text{s.t. } p + p_F \leq P_{\text{max}}, B + B_F \leq B_{\text{max}} \quad (28b)$$

$$p \geq 0, p_F \geq 0, B \geq 0, B_F \geq 0 \quad (28c)$$

$$\frac{d}{B_F \log \left(1 + \frac{p_F |h_F|^2}{B_F N_0} \right)} \leq \beta. \quad (28d)$$

It should be stressed that, in order to solve (28), it is not possible to employ the same approach used for rate maximization, because the presence of the denominator makes the logarithm of (28a) not jointly concave in all optimization variables. Moreover, standard fractional programming algorithms are not directly applicable since they have limited complexity only when the numerator and the denominator of the objective to maximize are concave and convex, respectively. Unfortunately, in (28), neither the concavity of the numerator, nor the convexity of the denominator hold. Finally, a third issue that makes (28) more challenging than the rate optimization problem is that, unlike the rate function, (28a) is not monotonically increasing in either p or p_F , and so it can not be guaranteed that, at the optimum, it holds $p + p_F = P_{\text{max}}$. On the other hand, (28a) is increasing in B and B_F , since, as shown in Section IV, the numerator is increasing in B and B_F , while the denominator depends only on B_F and decreases with B_F . Thus, at the optimum $B + B_F = B_{\text{max}}$ will hold. Exploiting this and defining

$$y = (B_{\text{max}} - B) \log \left(1 + \frac{p_F |h_F|^2}{(B_{\text{max}} - B) N_0} \right), \quad (29)$$

(28) can be cast as

$$\max_{p, B, p_F, y} \frac{(\beta - \frac{d}{y}) B \log \left(1 + \frac{p_F}{B} \right)}{\beta \mu p + P_c + \frac{d}{y} (\mu_F p_F - \mu p)} \quad (30a)$$

$$\text{s.t. } p + p_F \leq P_{\text{max}} \quad (30b)$$

$$0 \leq B \leq B_{\text{max}}, p \geq 0, p_F \geq 0 \quad (30c)$$

$$y = (B_{\text{max}} - B) \log \left(1 + \frac{p_F |h_F|^2}{(B_{\text{max}} - B) N_0} \right) \quad (30d)$$

$$y \geq \frac{d}{\beta}, \quad (30e)$$

wherein $P_c = NP_{c,n} + P_{c,0} + P_E$, and c is given in (15). Next, we also consider a relaxed version of (30) in which (30d) is reformulated into an inequality constraint, namely

$$\max_{p, B, p_F, y} \frac{(\beta - \frac{d}{y})B \log(1 + \frac{pc}{B})}{\beta \mu p + P_c + \frac{d}{y}(\mu_F p_F - \mu p)} \quad (31a)$$

$$\text{s.t. } p + p_F \leq P_{max} \quad (31b)$$

$$0 \leq B \leq B_{max}, p \geq 0, p_F \geq 0 \quad (31c)$$

$$y \leq (B_{max} - B) \log \left(1 + \frac{p_F |h_F|^2}{(B_{max} - B) N_0} \right) \quad (31d)$$

$$y \geq \frac{d}{\beta}, \quad (31e)$$

which, unlike (30), has a convex feasibility set, thanks to the fact that (30d) is an inequality constraint wherein the right-hand-side is a concave function. An important result is that, as shown in the coming proposition, (30) and (31) are equivalent problems.

Proposition 4: Problem (30) and (31) have the same set of optimal solutions.

Proof: The result follows by showing that any optimal solution of (31) is such that $y = (B_{max} - B) \log \left(1 + \frac{p_F |h_F|^2}{(B_{max} - B) N_0} \right)$. To this end, let us observe that (31a) is monotonically increasing in y . Indeed, by dividing numerator and denominator by $(\beta - \frac{d}{y})$, (31a) can be equivalently expressed as

$$\frac{B \log \left(1 + \frac{pc}{B} \right)}{\mu p + \frac{P_c y}{\beta y - d} + \frac{d \mu_F p_F}{\beta y - d}}, \quad (32)$$

which is strictly increasing in y . Based on this, the result follows proceeding by contradiction. Specifically, if \bar{y} were a solution of (31), but $y < (B_{max} - B) \log \left(1 + \frac{p_F |h_F|^2}{(B_{max} - B) N_0} \right)$, then it would be possible to find a feasible $y^* > \bar{y}$. Since (31a) is increasing in y , y^* would yield a larger objective value than \bar{y} , thus contradicting the fact \bar{y} is a solution of (31). ■

Despite having a convex feasibility set, Problem (31) is still challenging, since it does not lend itself to the use of fractional programming methods, due to the fact that the numerator and denominator of (31a) are not concave and convex functions, respectively. However, recalling also Lemma 2, they become respectively concave and convex if the variable y is fixed. More precisely, for any fixed y , Problem (31) is an instance of a so-called pseudo-concave maximization problem, in which the fraction to maximize has a concave numerator and an affine denominator, and thus can be solved with limited complexity by any fractional programming method, such as the popular Dinkelbach's method [50]. Moreover, from (31d) and (31e), it follows that y is

constrained to lie in the finite interval

$$y \in \left[\frac{d}{\beta}, B_{max} \log \left(1 + \frac{P_{max}|h_F|^2}{B_{max}N_0} \right) \right]. \quad (33)$$

Based on all of these considerations, Problem (31d) can be solved by performing a line search over y in the interval given by (33), and solving, for each considered value \tilde{y} , the corresponding pseudo-concave maximization problem as follows

$$\max_{p, B, p_F} \frac{(\beta - \frac{d}{\tilde{y}})B \log \left(1 + \frac{pc}{B} \right)}{\beta \mu p + P_c + \frac{d}{\tilde{y}}(\mu_F p_F - \mu p)} \quad (34a)$$

$$\text{s.t. } p + p_F \leq P_{max}, 0 \leq B \leq B_{max} \quad (34b)$$

$$p \geq 0, p_F \geq 0 \quad (34c)$$

$$(B_{max} - B) \log \left(1 + \frac{p_F |h_F|^2}{(B_{max} - B)N_0} \right) \geq \tilde{y} \quad (34d)$$

The formal algorithm is stated in Algorithm 2, wherein EE_m denotes the value of (34a) obtained at the m -th iteration.

Algorithm 2 EE Maximization

Set $M > 0$ and compute

$$\Delta = \frac{B_{max} \log \left(1 + \frac{P_{max}|h_F|^2}{B_{max}N_0} \right) - \frac{d}{\beta}}{M} \quad (35)$$

for $m = 1, \dots, M$ **do**

$$\tilde{y}_m = \frac{d}{\beta} + (m-1)\Delta;$$

Solve (34) and compute $EE_m(p_m^*, p_{m,F}^*, B_m^*, \tilde{y}_m)$

end for

Compute $m^* = \text{argmax } EE_m$;

Output $p_{m^*}^*, p_{m^*,F}^*, B_{m^*}^*, B_{m^*,F}^* = B_{max} - B_{m^*}^*$;

C. Rate-EE optimization

After having developed algorithms to optimize the system effective rate and energy efficiency, this section focuses on the bi-objective optimization problem that has as objectives both the rate and the energy efficiency functions, in order to characterize the rate-energy Pareto-optimal frontier of the considered RIS-based system.

To begin with, we observe that the allocation of $\Phi, \mathbf{q}, \mathbf{w}$ affects only the numerator of the energy efficiency, which coincides with the rate function in (1). Then, as far as the allocation of

$\Phi, \mathbf{q}, \mathbf{w}$ is concerned, there is no conflict between rate and the energy efficiency, and the same allocation of $\Phi, \mathbf{q}, \mathbf{w}$ can be used for both functions. Thus, we can plug any of the allocations of $\Phi, \mathbf{q}, \mathbf{w}$ developed in Section III into both the rate and the energy efficiency functions, which leads to the bi-objective problem

$$\max_{p, p_F, B} \{R(p, p_F, B, \Phi^{\text{opt}}, \mathbf{q}^{\text{opt}}, \mathbf{w}^{\text{opt}}), \text{EE}(p, p_F, B, \Phi^{\text{opt}}, \mathbf{q}^{\text{opt}}, \mathbf{w}^{\text{opt}})\} \quad (36a)$$

$$\text{s.t. } p + p_F \leq P_{\max} \quad (36b)$$

$$0 \leq B \leq B_{\max}, p \geq 0, p_F \geq 0 \quad (36c)$$

$$\frac{d}{(B_{\max} - B) \log \left(1 + \frac{p_F |h_F|^2}{(B_{\max} - B) N_0} \right)} \leq \beta, \quad (36d)$$

where we have already exploited the fact that at the optimum it must hold $B + B_F = B_{\max}$, since this is optimal for both the rate and the energy efficiency. On the other hand, with respect to the other variables, the rate and the energy efficiency functions are in general maximized by different resource allocations. Clearly, this is the scenario in which Problem (36) is of interest, because otherwise no trade-off would exist between the two functions, and the solution of Problem (36) would be trivially equal to the common maximizer of the rate and of the energy efficiency. Instead, when the maximizers of the rate and of the energy efficiency are different, simultaneously maximizing the rate and energy efficiency is not possible, which makes Problem (36) not trivial.

The most widely-used solution concept for bi-objective problems like (36) is that of Pareto-optimality. A Pareto-optimal solution of (36a) is a point lying on the so-called Pareto-frontier of the problem, defined as the set of resource allocations for which it is not possible to further increase either one of the two objectives, without decreasing the other objective. To elaborate further, let us denote by R_{opt} and EE_{opt} the maximum rate and energy efficiency that can be computed as shown in Sections IV-A and IV-B, respectively. Then, we also denote by $R_{\text{EE}_{\text{opt}}}$ the rate obtained with the resource allocation that maximizes the energy efficiency, and by $\text{EE}_{R_{\text{opt}}}$ the energy efficiency obtained with the resource allocation that maximizes the rate. Then, it can be seen that the extreme points of the Pareto-frontier in the $R - \text{EE}$ plane are $(R_{\text{opt}}, \text{EE}_{R_{\text{opt}}})$ and $(R_{\text{EE}_{\text{opt}}}, \text{EE}_{\text{opt}})$. As expected, this also shows that the Pareto-frontier degenerates into a single point when the rate and the energy efficiency admit the same maximizer. Instead, in general a non-trivial Pareto-frontier exists for (36), which provides all optimal trade-off points between the rate and the energy efficiency. Focusing on this scenario, multi-objective optimization theory

provides several approaches to compute all Pareto-optimal points of a multi-objective problem. One of the most widely-used methods is the maximization of the minimum between a weighted combination of the objectives. As for Problem (36), introducing the auxiliary variable y defined in (29), the max-min approach leads to considering the problem:

$$\max_{p, p_F, B, y} \min \left\{ \alpha \left(R(p, y, B, \Phi^{\text{opt}}, \mathbf{q}^{\text{opt}}, \mathbf{w}^{\text{opt}}) - R_{\text{opt}} \right), (1 - \alpha) \left(\frac{R(p, y, B, \Phi^{\text{opt}}, \mathbf{q}^{\text{opt}}, \mathbf{w}^{\text{opt}})}{\beta \mu p + P_c + \frac{d}{y} (\mu_F p_F - \mu p)} - \text{EE}_{\text{opt}} \right) \right\} \quad (37a)$$

$$\text{s.t. } p + p_F \leq P_{\max} \quad (37b)$$

$$0 \leq B \leq B_{\max}, p \geq 0, p_F \geq 0 \quad (37c)$$

$$\frac{d}{\beta} \leq y \leq (B_{\max} - B) \log \left(1 + \frac{p_F |h_F|^2}{(B_{\max} - B) N_0} \right) \quad (37d)$$

wherein we have plugged in the expression of the energy efficiency, with $R(p, y, B, \Phi^{\text{opt}}, \mathbf{q}^{\text{opt}}, \mathbf{w}^{\text{opt}}) = (\beta - \frac{d}{y}) B \log \left(1 + \frac{pc}{B} \right)$, α is a non-negative parameters that weighs the relative importance between the rate and the energy efficiency, while R_{opt} and EE_{opt} are the maximum of the rate and of the energy efficiency, respectively. For any $\alpha \in (0, 1)$, (37) has at least one solution that is Pareto-optimal for (37) [51, Theorem 3.4.3], and solving (37) for all $\alpha \in (0, 1)$ yields all the points on the Pareto-frontier of (36) [51, Theorem 3.4.5]. Also, the two extreme points $\alpha = 1$ and $\alpha = 0$ correspond to the single-objective maximization of the rate and of the energy efficiency.

In order to solve (37), we consider its equivalent reformulation in epigraph form, namely

$$\max_{p, p_F, B, y, t} t \quad (38a)$$

$$\text{s.t. } p + p_F \leq P_{\max} \quad (38b)$$

$$0 \leq B \leq B_{\max}, p \geq 0, p_F \geq 0 \quad (38c)$$

$$\frac{d}{\beta} \leq y \leq (B_{\max} - B) \log \left(1 + \frac{p_F |h_F|^2}{(B_{\max} - B) N_0} \right) \quad (38d)$$

$$\left(\beta - \frac{d}{y} \right) B \log \left(1 + \frac{pc}{B} \right) \geq \frac{t}{\alpha} + R_{\text{opt}} \quad (38e)$$

$$\left(\beta - \frac{d}{y} \right) B \log \left(1 + \frac{pc}{B} \right) \geq \left(\beta \mu p + P_c + \frac{d}{y} (\mu_F p_F - \mu p) \right) \left(\frac{t}{1 - \alpha} + \text{EE}_{\text{opt}} \right) \quad (38f)$$

Solving (37) is challenging due to the presence of the variable y . However, for any fixed y , (37) can be conveniently solved by employing the bisection algorithm over t , since all constraint

functions are convex in all other variables. Specifically, observing that y must lie in the interval defined by (33), Problem (38) can be solved by performing a line search over y , solving in each iteration the following problem with $y = \tilde{y}$ lying in in the interval defined by (33):

$$\max_{p, p_F, B, t} t \quad (39a)$$

$$\text{s.t. } p + p_F \leq P_{max} \quad (39b)$$

$$0 \leq B \leq B_{max}, p \geq 0, p_F \geq 0 \quad (39c)$$

$$(B_{max} - B) \log \left(1 + \frac{p_F |h_F|^2}{(B_{max} - B) N_0} \right) \geq \tilde{y} \quad (39d)$$

$$\left(\beta - \frac{d}{\tilde{y}} \right) B \log \left(1 + \frac{p_C}{B} \right) \geq \frac{t}{\alpha} + R_{opt} \quad (39e)$$

$$\left(\beta - \frac{d}{\tilde{y}} \right) B \log \left(1 + \frac{p_C}{B} \right) \geq \left(\beta \mu p + P_c + \frac{d}{\tilde{y}} (\mu_F p_F - \mu p) \right) \left(\frac{t}{1 - \alpha} + EE_{opt} \right) \quad (39f)$$

Then, Problem (37) can be solved similarly as in Algorithm 2. Formally, the approach is given in Algorithm 3.

Algorithm 3 Rate-EE Maximization

Set $M > 0$ and compute $\Delta = \frac{B_{max} \log \left(1 + \frac{P_{max} |h_F|^2}{B_{max} N_0} \right) - \frac{d}{\beta}}{M}$

for $m = 1, \dots, M$ **do**

$\tilde{y}_m = \frac{d}{\beta} + (m - 1)\Delta;$

Solve (39) by bisection over t and compute

$$F_m = \min \left\{ \alpha (R(p^*, p_F^*, B^*, \Phi^{opt}, \mathbf{q}^{opt}, \mathbf{w}^{opt}) - R_{opt}), (1 - \alpha) (EE(p^*, p_F^*, B^*, \Phi^{opt}, \mathbf{q}^{opt}, \mathbf{w}^{opt}) - EE_{opt}) \right\} \quad (40)$$

end for

Compute $m^* = \text{argmax } F_m;$

Output $p_{m^*}^*, p_{m^*, F}^*, B_{m^*}^*, B_{m^*, F}^* = B_{max} - B_{m^*}^*;$

V. NUMERICAL RESULTS

Consider the system model described in Section II, with system parameters set as in Table I. For all $nt = 1, \dots, N_T$, $nr = 1, \dots, N_R$, $n = 1, \dots, N$, each product channel has been generated as $h_{nt, n} g_{n, nr} = \frac{\alpha_h \alpha_g}{\sqrt{\beta}}$, wherein α_h and α_g are realizations of two independent complex circularly symmetric standard Gaussian variable, while β accounts for the overall path-loss and shadowing effects from the transmitter to the RIS and from the RIS to the receiver. In our simulations, we

| P_{max} | B_{max} | N_0 | μ | μ_F | $P_{c,0}$ | $P_{c,n}$ | b_F |
|-----------|-----------|-------------|-------|---------|-----------|-----------|---------|
| 45 dBm | 100 MHz | -174 dBm/Hz | 1 | 1 | 45 dBm | 10 dBm | 16 bits |

TABLE I: Network parameters

set $\beta = 10^{0.1*\beta_{dB}}$, with $\beta_{dB} = 110$. A similar model has been used to generate the feedback channel h_F .

Figure 1 plots the maximum spectral efficiency (rate normalized by B_{max}) versus N , with $N_T = N_R = 1$, $T_0 = 0.8 \mu s$ (Fig. 1-a), and $T_0 = 0.15 \mu s$ (Fig. 1-b), for the following schemes:

- (a) Optimization of p, p_F, B, B_F based on the optimal method from Sec. IV, with $\Phi = \mathbf{I}_N$, and \mathbf{q}, \mathbf{w} chosen as the dominant right and left eigenvectors of $\mathbf{A} = \mathbf{H}\Phi\mathbf{G}$. Thus, here the RIS simply reflects the signal without any phase manipulation. It is worth noting that in this case there is no need to configure the phase shifts of the RIS, and, therefore, the total overhead is much reduced. In particular, the numerical results that correspond to this case are obtained by setting $T_F = 0$ and $T_E = N_T N_R T_0$.
- (b) Optimization of p, p_F, B, B_F based on the optimal method from Sec. IV and of $\Phi, \mathbf{q}, \mathbf{w}$ based on the proposed method from Section III-A.
- (c) Optimization of p, p_F, B, B_F based on the optimal method from Section IV and of $\Phi, \mathbf{q}, \mathbf{w}$ based on the proposed method from Section III-B.
- (d) Optimization of p, p_F, B, B_F based on the optimal method from Section IV, and of $\Phi, \mathbf{q}, \mathbf{w}$ based on the alternating maximization Algorithm 1 from Section III-C.

The results in Figure 1 indicate that the proposed schemes are able to outperform the case in which no RIS optimization is performed, which shows that the use of RISs can significantly improve the system performance, even if the overhead for channel estimation and system configuration is taken into account. Moreover, it is seen that the proposed closed-form Schemes (b) and (c) offer similar performance as alternating optimization, which instead requires the implementation of an iterative numerical algorithm. Indeed, we recall that when $N_T = N_R = 1$, the closed-form Schemes (b) and (c) are provably optimal.

In order to show the impact of the overhead that is necessary to operate RIS-empowered wireless networks, Figure 2 considers a similar scenario as in Figure 1, with the only difference that the number of receive antennas is set to $N_R = 8$, which significantly increases the amount of feedback data. As a result, it is seen that the gap between Schemes (b), (c), (d), which optimize the phase shifts of the RIS, and Scheme (a) without RIS optimization, gets smaller, since not

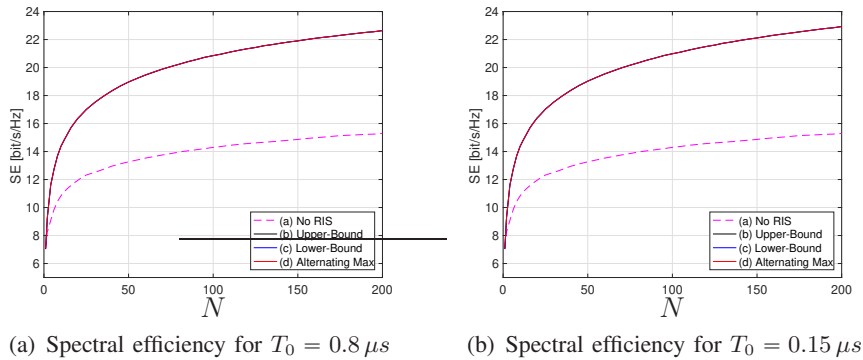


Fig. 1: Spectral efficiency as a function of N for $N_T = N_R = 1$.

optimizing the phases allows one to dispense with the overhead to obtain the channels \mathbf{H} and \mathbf{G} for each individual phase shift. Also, the gap is smaller when a larger T_0 is considered, since each pilot symbol needs more time. Moreover, it is interesting to observe that Scheme (b) performs like alternating optimization, despite requiring a much lower computational complexity thanks to the fact that it provides a closed-form allocation. On the other hand, Scheme (d) shows a slight gap compared to Schemes (b) and (d).

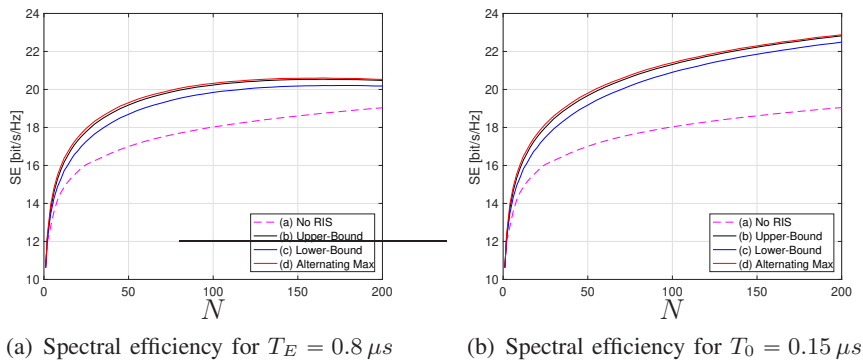
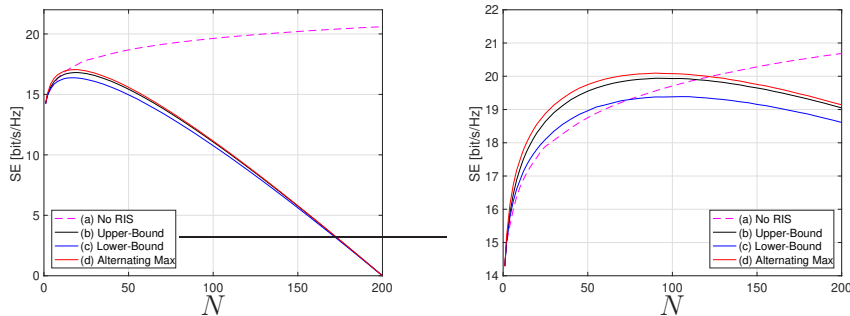


Fig. 2: Spectral efficiency as a function of N for $N_T = 1$, $N_R = 8$.

The trend displayed in Figure 2 becomes even more significant in Figure 3, where the number of antennas is further increased by considering that both the number of transmit and receive antennas is equal to $N_T = N_R = 8$. In this case, Scheme (a) which does not require any overhead for the optimization of the RIS phase shifts, outperforms the system setup in the presence of a RIS, when $T_0 = 0.8 \mu s$, i.e. when a longer time is used for channel estimation. Instead, when a shorter channel estimation time is used, i.e. when $T_0 = 0.15 \mu s$, performing radio resource allocation is still beneficial up to $N = 130$, whereas dispensing with resource

optimization, i.e. not using an RIS, becomes better for higher values of N . Moreover, also in this case it is observed how Schemes (b) and (d) perform very similarly, while Scheme (c) exhibits a slight performance gap.



(a) Spectral efficiency for large $T_0 = 0.8 \mu s$ (b) Spectral efficiency for small $T_0 = 0.15 \mu s$

Fig. 3: Spectral efficiency as a function of N for $N_T = 8$, $N_R = 8$.

The above results motivate the use of RISs in scenarios with a low number of transmit and receive antennas, especially for large N . Indeed, for any additional antenna that is deployed, N new channels must be estimated and the optimized phases need to be communicated to the RIS. In addition, comparing the performance of the optimized schemes in Figures 1 and 2, reveals that deploying a moderate number of antennas does not lead to improved performance. Indeed, the presence of an RIS already provides a large number of degrees of freedom, which make transmit beamforming and receive combining superfluous. This finding is in agreement with recent results available in [52].

Similar considerations hold for the case in which the energy efficiency is optimized, as it emerges from Figures 4, 5, 6, which consider the same four schemes considered in Figures 1, 2, 3, respectively, with the only differences that p, p_F, B, B_F have been allocated for energy efficiency maximization, according to the optimal method from Section IV-B, and that the performance metric that is reported is the energy efficiency, instead of the rate. Also, two values of P_0 are considered, namely $P_0 = 0.5 \text{ mW}$ and $P_0 = 2.5 \text{ mW}$.

In this case, Scheme (a) without any RIS feedback transmission starts performing better than the optimized schemes that rely on feedback transmissions when $N_R = 8$, $N_T = 1$, $T_0 = 0.8 \mu s$, and $N > 150$, i.e. for a lower overhead than for rate optimization. This can be explained since in the case of energy efficiency optimization, feedback overheads do not affect only the rate function, but also the power consumption at the denominator of the energy efficiency in (28a).

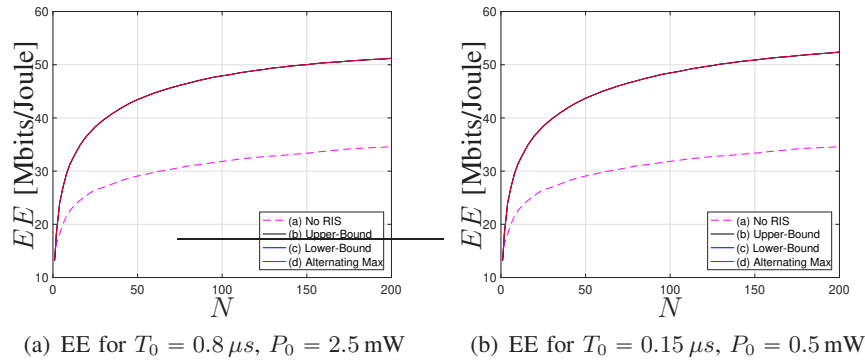


Fig. 4: Achieved EE in [Mbit/Joule] as a function of N for $N_T = N_R = 1$.

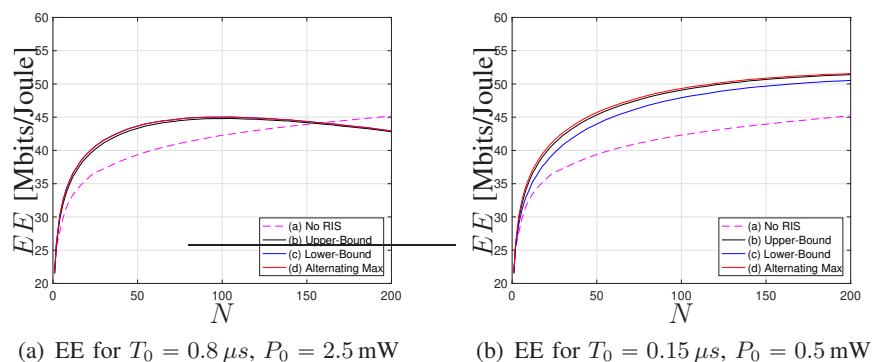


Fig. 5: Achieved EE in [Mbit/Joule] as a function of N for $N_T = 1$, $N_R = 8$.

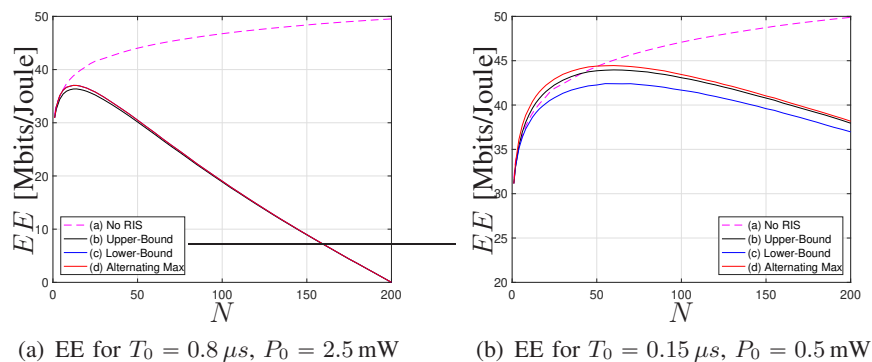


Fig. 6: Achieved EE in [Mbit/Joule] as a function of N for $N_T = 8$, $N_R = 8$.

Finally, Figures 7 and 8 consider again Schemes (a)-(d), with p, p_F, B, B_F allocated for rate-energy bi-objective maximization according to the optimal method from Section IV-C. The system rate-energy Pareto boundary is shown for the two cases: (1) $N_T = N_R = 1$; (2) $N_T = N_R = 8$, with $T_0 = 0.8 \mu s$. Similar remarks as for previous scenarios hold.

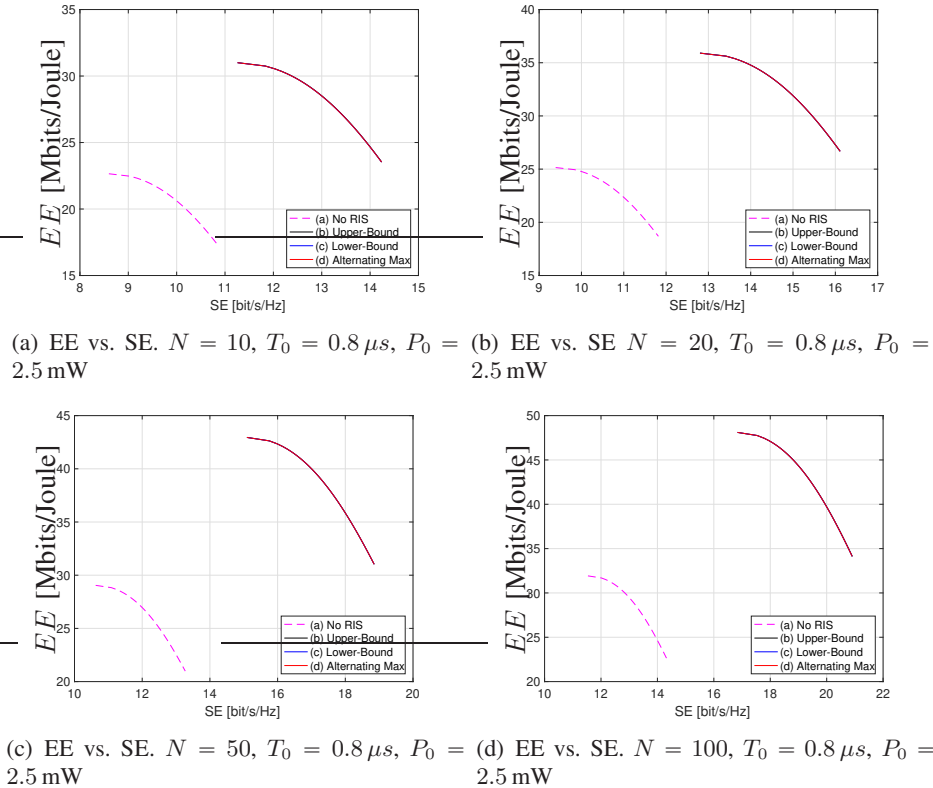


Fig. 7: Achieved EE in [Mbit/Joule] as a function of achieved SE [bits/s/Hz] for $N_T = N_R = 1$.

VI. CONCLUSIONS

A framework for overhead-aware radio resource allocation in RIS-based networks has been developed. The spectral and energy efficiencies have been optimized and the spectral-energy efficiency Pareto boundary has been characterized. Two new closed-form methods for the optimization of the RIS phase shifts, as well as of the transmit and receive filters, have been developed. Moreover, the transmit powers and bandwidths for the communication and feedback phases have been globally optimized through only concave/pseudo-concave maximizations.

The derived results indicate that RIS are particularly useful to provide new degrees of freedom when few transmit and receive antennas are deployed. Moreover, a clear trade-off exists between optimizing the network radio resources and the overhead that to deploy the optimized solution. In particular, a numerical analysis has shown that there exists a limit to the number of deployed antennas and number of RIS reflectors, before the feedback overhead makes radio resource optimization not convenient compared with the system setup where RISs are not deployed.

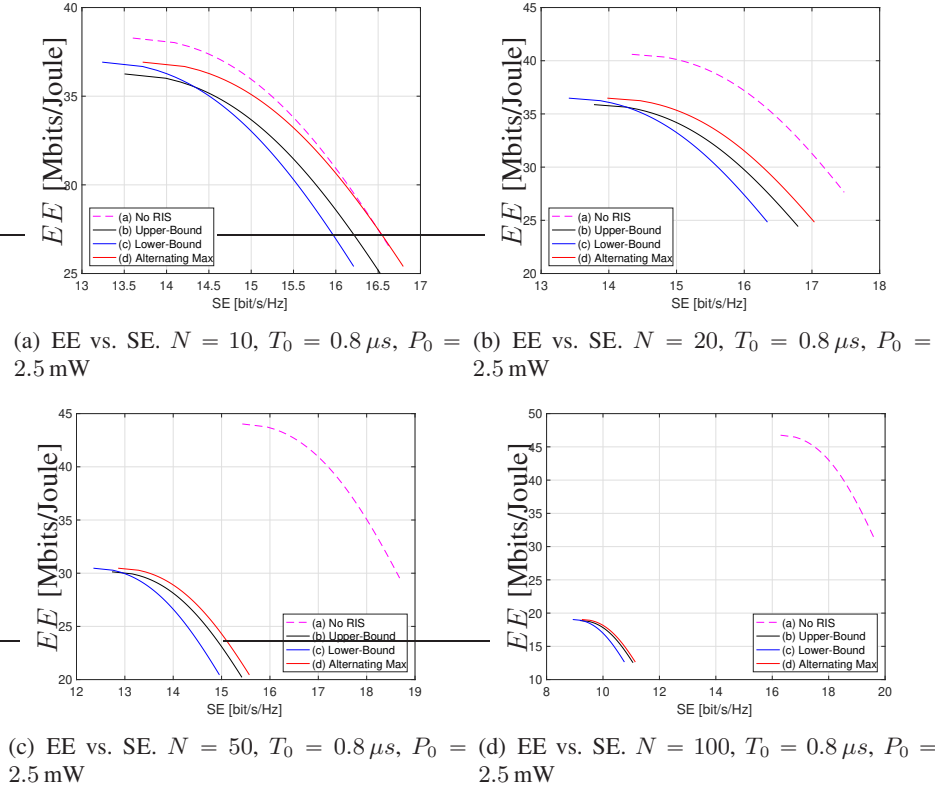


Fig. 8: Achieved EE in [Mbits/Joule] as a function of achieved SE [bit/s/Hz] with $N_T = 8$, $N_R = 8$.

REFERENCES

- [1] A. Gatherer, “What will 6G be?” <https://www.comsoc.org/publications/ctn/what-will-6g-be>, 2018.
- [2] J. G. Andrews, “Seven ways that hetnets are a cellular paradigm shift,” *IEEE Communications Magazine*, vol. 51, no. 3, pp. 136–144, 2013.
- [3] T. L. Marzetta, “Noncooperative cellular wireless with unlimited numbers of base station antennas,” *IEEE Transactions on Wireless Communications*, vol. 9, no. 11, pp. 3590–3600, 2010.
- [4] T. S. Rappaport *et al.*, “Millimeter wave mobile communications for 5G cellular: It will work!” *IEEE Access*, vol. 1, pp. 335–349, 2013.
- [5] J. Andrews, S. Buzzi, W. Choi, S. Hanly, A. Lozano, A. C. K. Soong, and J. C. Zhang, “What will 5G be?” *IEEE Journal on Selected Areas in Communications*, vol. 32, no. 6, pp. 1065–1082, June 2014.
- [6] 5G PPP, “5GPPP vision on software networks and 5G SN WG,” https://5g-ppp.eu/wp-content/uploads/2014/02/5G-PPP_SoftNets_WG_whitepaper_v20.pdf, 2017.
- [7] P. Popovski, K. F. Trillingsgaard, O. Simeone, and G. Durisi, “5G wireless network slicing for eMBB, URLLC, and mMTC: A communication-theoretic view,” *IEEE Access*, vol. 6, pp. 55 765–55 779, 2018.
- [8] A. Zappone, M. Di Renzo, and M. Debbah, “Wireless networks design in the era of deep learning: Model-based, AI-based, or both?” *IEEE Transactions on Communications*, vol. 67, no. 10, pp. 7331–7376, October 2019.
- [9] L. Subrt and P. Pechac, “Controlling propagation environments using intelligent walls,” *European Conference on Antennas and Propagation*, 2012.

- [10] M. Di Renzo *et al.*, “Smart radio environments empowered by reconfigurable AI meta-surfaces: An idea whose time has come,” *EURASIP Journal on Wireless Communications and Networking*, vol. 129, 2019.
- [11] N. Yu, P. Genevet, M. A. Kats, F. Aieta, J.-P. Tetienne, F. Capasso, and Z. Gaburro, “Light propagation with phase discontinuities: Generalized laws of reflection and refraction,” *Science*, vol. 334, no. 6054, pp. 333–337, 2011.
- [12] F. Liu *et al.*, “Programmable metasurfaces: State of the art and prospects,” *IEEE International Symposium on Circuits and Systems*, 2018.
- [13] C. Liaskos *et al.*, “Realizing wireless communication through software-defined hypersurface environments,” *IEEE International Symposium on World of Wireless, Mobile and Multimedia Networks*, 2018.
- [14] M. D. Renzo *et al.*, “Analytical modeling of the path-loss for reconfigurable intelligent surfaces - anomalous mirror or scatterer,” <https://arxiv.org/pdf/2001.10862.pdf>, 2020.
- [15] V. S. Asadchy, M. Albooyeh, S. N. Tcvetkova, A. Diaz-Rubio, Y. Radi, and S. A. Tretyakov, “Perfect control of reflection and refraction using spatially dispersive metasurfaces,” *Physical Review B*, vol. 94, no. 7, 2016.
- [16] A. Diaz-Rubio, V. S. Asadchy, A. Elsakka, and S. A. Tretyakov, “From the generalized reflection law to the realization of perfect anomalous reflectors,” *Science Advances*, vol. 3, no. 8, 2017.
- [17] C. Liaskos, S. Nie, A. Tsioliariidou, A. Pitsillides, S. Ioannidis, and I. F. Akyildiz, “A new wireless communication paradigm through software-controlled metasurfaces,” *IEEE Communications Magazine*, vol. 56, no. 9, pp. 162–169, 2018.
- [18] Q. Wu and R. Zhang, “Towards smart and reconfigurable environment: Intelligent reflecting surface aided wireless network,” *IEEE Communications Magazine*, 2019.
- [19] E. Basar *et al.*, “Wireless communications through reconfigurable intelligent surfaces,” *IEEE Access*, vol. 7, pp. 116 753–116 773, 2019.
- [20] C. Huang *et al.*, “Holographic MIMO surfaces for 6G wireless networks: Opportunities, challenges, and trends,” <https://arxiv.org/pdf/1911.12296.pdf>, 2019.
- [21] S. Hu, F. Rusek, and O. Edfors, “Beyond massive mimo: The potential of data transmission with large intelligent surfaces,” *IEEE Transactions on Signal Processing*, vol. 66, no. 10, pp. 2746–2758, May 2018.
- [22] N. Shlezinger, O. Dicker, Y. C. Eldar, I. Yoo, M. F. Imani, and D. R. Smith, “Dynamic metasurface antennas for uplink massive mimo systems,” *IEEE Transactions on Communications*, vol. 67, no. 10, pp. 6829–6843, October 2019.
- [23] M. Di Renzo *et al.*, “Reconfigurable intelligent surfaces vs. relaying: Differences, similarities, and performance comparison,” <https://arxiv.org/abs/1908.08747>, 2019.
- [24] X. Lu, E. Hossain, T. Shafique, S. Feng, H. Jiang, and D. Niyato, “Intelligent reflecting surface (IRS)-enabled covert communications in wireless networks,” <https://arxiv.org/abs/1911.00986>, 2019.
- [25] N. Kaina, M. Dupre, G. Lerosey, and M. Fink, “Shaping complex microwave fields in reverberating media with binary tunable metasurfaces,” *Scientific Reports, Article ID 6693*, vol. 4, 2014.
- [26] G. Lavigne *et al.*, “Susceptibility derivation and experimental demonstration of refracting metasurfaces without spurious diffraction,” *IEEE Transactions on Antennas and Propagation*, vol. 66, no. 3, pp. 1321–1330, 2018.
- [27] W. Tang, X. Li, J. Y. Dai, S. Jin, Y. Zeng, Q. Cheng, and T. J. Cui, “Wireless communications with programmable metasurface: Transceiver design and experimental results,” *China Communications*, vol. 16, no. 5, pp. 46–61, May 2019.
- [28] W. Tang, J. Y. Dai, M. Chen, X. Li, Q. Cheng, S. Jin, K.-K. Wong, and T. J. Cui, “Programmable metasurface-based RF chain-free 8PSK wireless transmitter,” *IEEE Electronic Letters*, vol. 55, no. 7, pp. 417–420, 2019.
- [29] L. Dai *et al.*, “Reconfigurable intelligent surface-based wireless communication: Antenna design, prototyping and experimental results,” <https://arxiv.org/pdf/1912.03620.pdf>, 2019.
- [30] C. Huang, A. Zappone, G. C. Alexandropoulos, M. Debbah, and C. Yuen, “Reconfigurable intelligent surfaces for energy efficiency in wireless communication,” *IEEE Trans. on Wireless Commun.*, vol. 18, no. 8, pp. 4157–4170, 2019.

- [31] Q. Wu and R. Zhang, "Intelligent reflecting surface enhanced wireless network: Joint active and passive beamforming design," *IEEE Transactions on Wireless Communications*, vol. 18, no. 11, pp. 5394–5409, November 2019.
- [32] Y. Yang, S. Zhang, and R. Zhang, "IRS-enhanced OFDM: Power allocation and passive array optimization," <https://arxiv.org/pdf/1905.00604.pdf>, 2019.
- [33] X. Yu, D. Xu, and R. Schober, "MISO wireless communication systems via intelligent reflecting surfaces," in *2019 IEEE/CIC International Conference on Communications in China (ICCC)*, 2019.
- [34] H. Guo, Y.-C. Liang, J. Chen, and E. G. Larsson, "Weighted sum-rate optimization for intelligent reflecting surface enhanced wireless networks," <https://arxiv.org/pdf/1905.07920.pdf>, 2019.
- [35] T. Jiang and Y. Shi, "Over-the-air computation via intelligent reflecting surfaces," <https://arxiv.org/pdf/1904.12475.pdf>, 2019.
- [36] J. Chen, Y.-C. Liang, Y. Pei, and H. Guo, "Intelligent reflecting surface: A programmable wireless environment for physical layer security," *IEEE Access*, vol. 7, pp. 82 599–82 612, June 2019.
- [37] M. Cui, G. Zhang, and R. Zhang, "Secure wireless communication via intelligent reflecting surface," *IEEE Wireless Communication Letters*, vol. 8, no. 5, pp. 1410–1414, October 2019.
- [38] H. Shen, W. Xu, S. Gong, Z. He, and C. Zhao, "Secrecy rate maximization for intelligent reflecting surface assisted multi-antenna communications," *IEEE Communications Letters*, vol. 23, no. 9, pp. 1488–1492, September 2019.
- [39] X. Li, J. Fang, F. Gao, and H. Li, "Joint active and passive beamforming for intelligent reflecting surface-assisted massive MIMO systems," <https://arxiv.org/abs/1912.00728>, 2019.
- [40] D. Ma, M. Ding, and M. Hassan, "Enhancing cellular communications for UAVs via intelligent reflective surface," <https://arxiv.org/abs/1911.07631>, 2019.
- [41] R. Liu, H. Li, M. Li, and Q. Liu, "Symbol-level precoding design for intelligent reflecting surface assisted multi-user MIMO systems," <https://arxiv.org/abs/1909.01015>, 2019.
- [42] B. Ning, Z. Chen, W. Chen, and J. Fang, "Intelligent reflecting surface design for MIMO system by maximizing sum-path-gains," <https://arxiv.org/abs/1909.07282>, 2019.
- [43] H. Han *et al.*, "Intelligent reflecting surface aided network: Power control for physical-layer broadcasting," <https://arxiv.org/abs/1910.14383>, 2019.
- [44] C. Pan, H. Ren, K. Wang, W. Xu, M. Elkashlan, A. Nallanathan, and L. Hanzo, "Multicell MIMO communications relying on intelligent reflecting surface," <https://arxiv.org/abs/1907.10864>, 2019.
- [45] P. Wang, J. Fang, X. Yuan, Z. D. Chen, H. Duan, and H. Li, "Intelligent reflecting surface-assisted millimeter wave communications: Joint active and passive precoding design," <https://arxiv.org/abs/1908.10734>, 2019.
- [46] C. You, B. Zheng, and R. Zhang, "Intelligent reflecting surface with discrete phase shifts: Channel estimation and passive beamforming," <https://arxiv.org/abs/1911.03916>, 2019.
- [47] R. A. Horn and C. R. Johnson, *Topics in Matrix Analysis*. Cambridge University Press, 1991.
- [48] Z.-Q. He and X. Yuan, "Cascaded channel estimation for large intelligent metasurface assisted massive MIMO," *IEEE Wireless Communication Letters*, vol. 9, no. 2, pp. 210–214, February 2019.
- [49] S. P. Boyd and L. Vandenberghe, *Convex optimization*. Cambridge Univ Press, 2004.
- [50] W. Dinkelbach, "On nonlinear fractional programming," *Management Science*, vol. 13, no. 7, pp. 492–498, March 1967.
- [51] K. Miettinen, *Nonlinear Multiobjective Optimization*. Springer, 1999.
- [52] V. Arun and H. Balakrishnan, "RFocus: Practical beamforming for small devices," <https://arxiv.org/abs/1905.05130>, 2019.